# Carbon epoxy composites thermal conductivity at 80 K and 300 K

J.-L. Battaglia, M. Saboul, J. ~~Pahlies~~Pailhes, A. Saci, O. Fudym

Laboratory I2M, University of Bordeaux

jl.battaglia@i2m.u-bordeaux1.fr

## I. Introduction

The ~~new micro~~satellite launchers technology with liquid or hybrid propulsion needs very light devices including the ~~oxygen~~ cryogenic tank~~-~~ that are one of the most part of the complete system. Whereas metals were extensively used as tank materials[1,2], the composite technology appears more promising but also raises new technological challenges. The main one is related to its compability with the liquid ergol. ~~to t~~The ignition and combustion of the carbon-epoxy material in contact with the liquid oxygen[3] is a part of this challenge~~.~~ The oxygen tank pressure[4], the oxygen concentration[5,6,7], and temperature[8] are keys parameters in the ignition and combustion processes. Temperature increase can be originated from multiple phenomena as: a particle impact[1], a fast liquid compression[9], friction[1] between liquid and solid wall or mechanical resonance due to vibrations[1]. The main drawback of composites is their low performance with respect to combustion. The process of polymer matrix decomposition is the major factor to trigger the ignition. However the fiber is also highly responsible in the heat transfer within the heating area. Gerzeski[10] found that most of metallic materials (aluminium alloys, nickel) satisfies the mechanical impact test due to their high thermal conductivity at temperature of -196 ° C (77K). This has led to the development of composite materials with the same resin, and different fibers[10,11,12]. Therefore, composites capable of meeting the compatibility liquid oxygen standard must have high ignition temperature of the resin and a high thermal conductivity of the composite, and therefore of the fiber.

This study focuses on the thermal conductivity measurement of three composites constituted from the same epoxy resin (5052-4 RTM BMI) and different carbon fibers, namely the XN15, YSH70 and CN90. Each composites samples are removed from a plate in the form of cylindrical samples of $R$=1.5 cm and thickness $e$=3 mm. Each sample is constituted from the same number of folds (about 40) and the ~~winding~~ process lead to orientate the fibers in the [-45, 0, 45, 90]°, which allows to assume homogenous In-plane properties. The measured density of the fibers and the resin are reported in Tab. 1. As reported in the paper of Reed and Golda[14], epoxy resins contract from 0.85 to 1.2 % on cooling from 300 to 4K. Therefore the density will be further considered as a constant on the [300-77] K temperature range. On the other hand, the coefficient thermal expansion in the same temperature range is lower than $0.5 \times 10^{-6}$ $K^{-1}$. Therefore, the fiber density will be considered as a constant. The measured composite density differs less than 4% from the calculated value starting from the fiber volume fraction. It means that the volume fraction is slightly higher than the real value.

Mis en forme : Exposant

As reported in [13,14], the specific heat of epoxy is 1110 $J.kg^{-1}.K^{-1}$ at 300 K and it is about 380 $J.kg^{-1}.K^{-1}$ à 77 K. In addition, the specific heat of graphite is[15] 644 $J.kg^{-1}.K^{-1}$ at 300 K and it is about 109 $J.kg^{-1}.K^{-1}$ at 77 K.

The specific heat of the composite has been measured at 300 K and it is calculated starting from the fiber volume fraction $f$. The results are reported in the first column of Tab. 2. A very slight difference (less than 2%) appears that comes, as also reported for the density, from a very small overestimation of the fiber volume fraction. The specific heat of the composite at

77 K is then calculated starting from the values for the carbon fiber and the resin at that temperature and also from the fiber volume fraction with 2% correction term. Results are reported in the second column of Tab. 2.

| Composite | Fiber density ($kg.m^{-3}$) @300K/77K | Resin density ($kg.m^{-3}$) @300K/77K | Fiber longitudinal thermal conductivity $k_f$ ($W.m^{-1}.K^{-1}$) @300K | Fiber volume fraction *f* | Composite density ($kg.m^{-3}$) @300K Meas./Calc. |
|---|---|---|---|---|---|
| XN15/Epoxy | 1850 | 1210 | 3.2 | 0.568 | 1516/1573 |
| YSH70/Epoxy | 2150 | 1210 | 250 | 0.586 | 1783/1760 |
| CN90/Epoxy | 2190 | 1210 | 400 | 0.609 | 1788/1807 |

**Tab. 1**. Measured density of the fiber and the resin at 300 K and 77 K, measured thermal conductivity of the fiber at 300K and measured composite density at 300 K with comparison with the calculated one.

| $T_0$ [K] | XN 15/epoxy | YSH 70/epoxy | CN 90/epoxy |
|---|---|---|---|
| 300 (measured/calculated) | 836/845 | 829/836 | 817/826 |
| 77 (calculated with 2% correction) | 232 | 228 | 219 |

**Tab. 2**. Measured/calculated specific heat in [$J.K^{-1}.kg^{-1}$] of the three composites at 300 K. Calculated value at 77 K with 2% correction term coming from the fiber volume fraction overestimation.

The In-plane $k_{||}$ and transverse $k_{\perp}$ thermal conductivity are measured at 77K and 300K using the hot disk technique. The thermal resistance $R_c$ at the interface between the probe and the material is a key parameter that needs also to be identified as well as for the heat capacity of the probe. An inverse technique is implemented that lead to identify the unknown parameters based on experimental data and a heat transfer model consistent with the experiment. For information[16,17], the longitudinal thermal conductivity of the fibers at 300 K is reported in Tab. 1 and the thermal conductivity $k_r$ of the epoxy resin is 0.1 $W.m^{-1}.K^{-1}$ at 80 K and it is 0.25 $W.m^{-1}.K^{-1}$ at ~~0.25~~300 K.

## II. Thermal conductivity measurements

In-plane and transverse thermal conductivity of the composite are measured using a hot probe type method known as the hot disk technique[18,19,20,21]. The sensor is made of nickel foil in the form of a bifilar spiral covered on both sides with an insulating layer of Kapton. The thicknesses of the foil and the Kapton layer are 10 and 25 µm, respectively, the effective diameter of the bifilar spiral is $r_0 = 3.189\,\text{mm}$ and the radius of the heating area is 20 mm.

Code de champ modifié
Code de champ modifié
Code de champ modifié

The thermal sensor is placed between two pieces of the sample material and is then heated by a constant electrical current *i*. The probe constitutes both heat source and temperature sensor. The time-dependent resistance of the thermal probe sensor element, during the transient recording, is expressed as:

$$R(t) = R_0(T_0)\left(1 + a(T_0)\Delta T(t)\right) \quad (1)$$

Code de champ modifié

where $R_0$ is the resistance of the probe element at the initial temperature $T_0$, $a(T_0)$ is the temperature coefficient of resistance (TCR) that is calibrated prior to the experiment and $\Delta T(t)$ is the temperature increase of the probe during the heating.

The probe resistance $R_0$ and TCR $\alpha$ have been accurately measured for the temperature range of interest and data are reported in Tab. I.

Classical assumptions are that the heat flux related to the Joule's effect is uniform all over the probe area at each time $t$ during the experiment and that it is measured the average temperature $\overline{T}$ of the probe.

| $T_0$ [K] | $R_0$ ($T_0$) [Ω] | $\alpha(T_0)$ [$K^{-1}$] x $10^{-3}$ |
|---|---|---|
| 80 | 1.049 | 11.593 |
| 300 | 5.313 | 5.098 |

Tab. 3. Probe resistance and TCR at 80 K and 300 K.

To record the potential difference variations at the sensor, which normally are of the order of a few millivolts during the transient recording, a bridge arrangement is used in order to have a current $i$ holding constant through the probe.

Heat diffusion in the sample rests on the classical linear heat diffusion equation in cylindrical coordinates. Heat flux $j_0/2 = R_0 i^2/2$ is imposed at one face of the sample by the thermal probe, whereas the temperature at the other face is maintained at the constant value $T_0$. It is finally assumed that the circumference area is perfectly insulated (in practice, the heating duration is chosen so that heat diffusion length does not exceed the sample radius $R$).
Using the experimental symmetry, it is allowed to consider only one of the two samples located at both sides of the thermal probe. Applying the Laplace transform on the time variable and the Hankel transform on the radial coordinate, an analytical expression for the spatial average sensor temperature $\overline{T}(t)$ is found as:

$$\overline{T}(t) = L^{-1}\left(Z(p)\right)\frac{j_0}{2} \tag{2}$$

Code de champ modifié

In this relation $p$ denotes the Laplace variable and $L^{-1}(\ )$ is the inverse Laplace transform that is calculated from the de Hoog algorithm. The transfer function $Z(p)$ is given by :

$$Z(p) = \frac{1}{p}\left(\frac{1}{C_s p + \dfrac{1}{R_c + F(p)}}\right), \tag{3}$$

Code de champ modifié

where $C_s$ is the probe heat capacity that leads to a delay in the thermal response and $R_c$ is the thermal contact resistance at the interface between the probe and the sample. Function $F(p)$ is given by:

$$F(p) = \left(\frac{r_0}{R}\right)^2 F_0(a_0, p) + \sum_{n=1}^{N} F_0(a_n, p)\frac{4\left[J_1(a_n r_0)\right]^2}{R^2 a_n^2\left[J_0(a_n R)\right]^2}, \tag{4}$$

Code de champ modifié

where $J_0(\ )$ and $J_1(\ )$ are the first and second order Bessel functions of second specie and:

$$F_0(a_n,p)=\frac{1-e^{-2b_n e}}{b_n k_\wedge\left(1+e^{-2b_n e}\right)} \quad (5)$$

Code de champ modifié

With:

$$\beta_n=\sqrt{a_n^2\frac{k_{\|}}{k_\perp}+\frac{p\rho_c C_{p_c}}{k_\perp}} \quad (6)$$

Code de champ modifié

And:

$$a_n=\begin{cases}0 \text{ if } n=0\\ p\left(n+\frac{1}{4}\right)-\frac{3}{8p\left(n+\frac{1}{4}\right)R} \text{ if } n=1,2,3,...\end{cases} \quad (7)$$

Code de champ modifié

In addition of the two thermal conductivity $k_{\|}$ and $k_\wedge$, the probe capacity $C_s$ and the thermal resistance $R_c$ at the probe-sample interface are unknown. In order to assess the identification feasibility, the dimensionless sensitivity functions $X_q(t)=q\left[\mathrm{d}\overline{T}(t)/\mathrm{d}q\right]$ for the four parameters $\theta=\left[k_{\|},k_\perp,R_c,C_s\right]$ are calculated and plotted in Fig. 1.

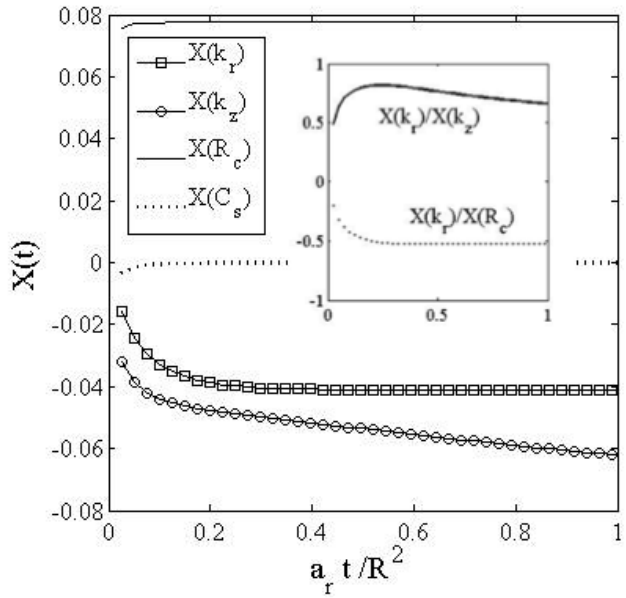


**Fig. 1**. Dimensionless sensitivity for $k_{\|}$, $k_\wedge$, $R_c$ and $C_s$ according to $a_r t/R^2$. Numerical values for this simulation are: $R$=1.5 cm, $e$=3mm, $k_{\|}=100$ W.m$^{-1}$.K$^{-1}$, $k_\wedge=3$W.m$^{-1}$.K$^{-1}$, $R_c=10^{-4}$K.m$^2$.W$^{-1}$, $C_s=20$ J.K$^{-1}$.m$^{-2}$.

The sensitivity functions for the two thermal conductivities are not fully linear dependant (as also demonstrated by plotting their ratio in the inset of the figure). The sensitivity for $C_s$ is close to zero on the quasi-total time range. Finally the sensitivity of the $R_c$ varies only at the short times and then remains constant. As represented in the inset of the figure, the sensitivity functions for $k_r$ and $R_c$ are linear independant only at the first instants, which ~~com~~requires to identify both parameters separately considering the first part of the data.
Therefore, $C_s$ is measured from an experiment with the probe alone at the two investigated temperatures (330 K and 77 K), for a given time step. It is found $C_s = 26 \pm 0.5$ J.K$^{-1}$.m$^{-2}$ at 300 K and $C_s = 20 \pm 0.5$ J.K$^{-1}$.m$^{-2}$ at 77 K and it is assumed that those values do not change significantly when the probe is inserted between both parts of the composite.

## III. Results

The sampling time interval is noted $\Delta t$ and the number of data is $N$ for the duration of the experiment. The four parameters have been identified minimizing the objective function $J = \sum_{i=1}^{N} e_i^2 = \sum_{i=1}^{N} \left( Y_i - \overline{T}_i \right)^2$, i.e., the quadratic difference~~gap~~ between the measured temperature $Y_i = Y(i\Delta t)$ and the simulated one $\overline{T}_i$ obtained from relation (2)~~(2)~~. The minimization is achieved using the Levenberg-Marquardt algorithm. Results are reported in Tab. II. The measured temperature and the simulated one starting from the identified parameters are plotted in Fig. II.

**Mis en forme :** Police :(Par défaut) Times New Roman, Anglais (Royaume-Uni)

The fit between measures and simulations is almost perfect; the residuals are low with a white~~with~~ noise featuring (the auto-correlation function being close to a Dirac function). The value of the objective function at the end of the identification process is less than $10^{-5}$ and the residuals do not reveal a bias in the heat transfer model. The standard deviations for the identified parameters are classically calculated from: $\sigma_q = \sqrt{\left(\mathbf{X}^T \mathbf{X}\right)^{-1} \sigma_{\overline{T}}^2}$ with $\mathbf{X} = \left[ \mathbf{X}(k_r) \;\; \mathbf{X}(k_z) \;\; \mathbf{X}(R_c) \;\; \mathbf{X}(C_s) \right]$ where $\mathbf{X}(q)$ denotes the sensitivity vector, of length $N$, for $q = \left[ k_r, k_z, R_c, C_s \right]$. Furthermore, the noise standard deviation is approximated from the value of the objective function $J_{\min}$ at the end of the identification process as: $\sigma_{\overline{T}}^2 = J_{\min} / N$.

| XN 15/epoxy | | | |
|---|---|---|---|
| $T_0$ [K] | $k_{\parallel}$ [W.m$^{-1}$.K$^{-1}$] | $k_{\perp}$ [W.m$^{-1}$.K$^{-1}$] | $R_c$ [m$^2$.K.W$^{-1}$] |
| 77 | $0.479 \pm 0.051$ | $0.203 \pm 0.005$ | $(5.231 \pm 0.210)$x10$^{-4}$ |
| 300 | $1.794 \pm 0.030$ | $0.886 \pm 0.004$ | $(4.409 \pm 0.100)$x10$^{-4}$ |
| YSH 10/epoxy | | | |
| 77 | $28.02 \pm 0.25$ | $0.168 \pm 0.020$ | $(1.400 \pm 0.10)$x10$^{-4}$ |
| 300 | $152.78 \pm 0.90$ | $0.456 \pm 0.020$ | $(3.699 \pm 0.30)$x10$^{-4}$ |
| CN 90/epoxy | | | |
| 77 | $49.85 \pm 0.91$ | $0.324 \pm 0.035$ | $(4.032 \pm 0.10)$x10$^{-4}$ |
| 300 | $230.22 \pm 1.20$ | $0.602 \pm 0.030$ | $(4.429 \pm 0.20)$x10$^{-4}$ |

**Tab. 4**. Identified In-plane and transverse thermal conductivity and thermal resistance at the interface between the material and the probe.

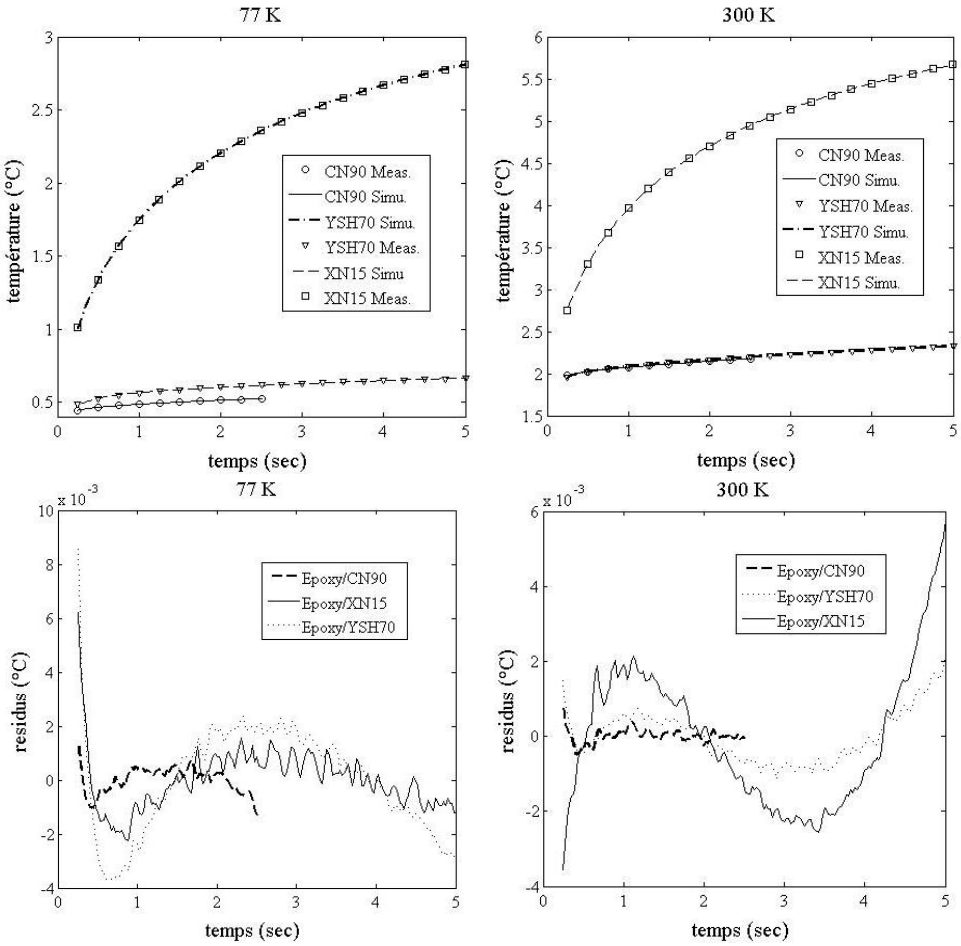


**Fig. 2**. First row: measured temperature $Y(t)$ during the transient hot disk experiment and simulated temperature $\overline{T}(t)$ with identified parameters reported in Tab. 4 at 77 K and 300 K. Second row: residuals $e(t)$ .

## IV. Conclusions

The measured In-plane thermal conductivity of the three composites follows well the carbon fibre longitudinal thermal conductivity at room temperature. Obviously, the epoxy resin being less conductive than the fibre, the composite thermal conductivity is lower than that of the fibre itself. Using the classical mixing law for the in plane thermal conductivity it is found the theoretical value as: $k_{\parallel} = f\,k_f + (1-f)k_r$. Using the fibre volume fraction, the longitudinal thermal conductivity of the fibre at 300 K in Tab. 1 and that of the resin at 300 K, we found the theoretical value of $k_{\parallel}$ for the three composites at 300 K as: $k_{\parallel}^{th} = 1.925\,\mathrm{W.m^{-1}.K^{-1}}$ for the

XN15/epoxy, $k_{\parallel}^{th} = 146.6\,\mathrm{W.m^{-1}.K^{-1}}$ for the YSH10/epoxy and $k_{\parallel}^{th} = 243\,\mathrm{W.m^{-1}.K^{-1}}$ for the CN90/epoxy. These values are consistent with the measured ones reported in Tab. 4. Using the measured values at 77 K, it comes that the thermal conductivity of the carbon fiber can be estimated from the previous mixing law and the epoxy thermal conductivity at 77 K. We found: $k_{\mathrm{XN15,77K}} = 0.76\,\mathrm{W.m^{-1}.K^{-1}}$, $k_{\mathrm{YSH70,77K}} = 47.74\,\mathrm{W.m^{-1}.K^{-1}}$ and $k_{\mathrm{CN90,77K}} = 81.77\,\mathrm{W.m^{-1}.K^{-1}}$. Ignition test realized on the three composites showed that only the CN90/epoxy passed the test. This suggests that the thermal conductivity of carbon/epoxy material for liquid oxygen storage purpose must be equal or greater than $k_{\parallel}^{\min} = 50\,\mathrm{W.m^{-1}.K^{-1}}$.


[1] K. R. Rosales, *Guide for Oxygen Compatibility Assessments on Oxygen Components and Systems*, NASA/TM-2007-213740, 2007.

[2] E. Zawierucha, A. V. Samant and J. F. Million, *Promoted Ignition-Combustion behaviour of cast and wrought engineering alloys in oxygen-enriched atmospheres*, Flammability and Sensitivity of materials in oxygen-enriched atmospheres, ASTM STP 1454, **10** (2003).

[3] R. Kim, C. W. Lee, J. Camping, K. B. Bowman, *Impact reaction of composites in Liquid Oxygen*, American Institute of Aeronautics and Astronautics, **10**, 2005-2158 (2005).

[4] C. J. Bryan, *Ignitability in air, gaseous oxygen and oxygen-enriched environments of polymers used in breathing-air devices - final report*, "Flammability and Sensitivity of materials in oxygen-enriched atmospheres", American Society for Testing and Materials STP 1395, **9** (2000).

[5] G. Wang, X. Li, R. Yan and S. Xing, *The study on compatibility of polymer matrix resins with liquid oxygen*, Materials Science and Engineering B, **132**, N° 1-2 (2006).

[6] D. Hirsch, R. Bunker and D. Janoff, *Effects of oxygen concentration, diluents and pressure on ignition and flame-Spread rates of nonmetals*: *A review paper*, "Flammability and Sensitivity of materials in oxygen-enriched atmospheres", American Society for Testing and Materials STP 1111, **5** (1991).

[7] F.-Y. Hshieh and H. Beeson, *Flammability testing of flame-retarded epoxy composites and phenolic composites*, Fire and materials, **21** (1997).

[8] H. Barthélémy, G. Deloge and V. Gérard, *Ignition of materials in oxygen atmospheres: comparison of different testing methods for ranking materials*, "Flammability and Sensitivity of materials in oxygen-enriched atmospheres", American Society for Testing and Materials STP 1111, **5** (1991).

[9] L. Dequay and P. Sheuermann, *Analysis of oxygen mechanical impact test apparatuses and methods*, "Flammability and Sensitivity of materials in oxygen-enriched atmospheres", American Society for Testing and Materials STP 1111, **5** (1991).

[10] R. Gerzeski, *LOX Compatible toughened bismaleimide matrix thermally conductive fibre composites, Part 1: Composite fabrication viability and thermal conductivity measurement*, Journal of testing and evaluation **36**, N° 1 (2008).

[11] R. Gerzeski, *LOX Compatible toughened bismaleimide matrix thermally conductive fibre composites, Part 2: ASTM D2512 Specimen fabrication, cleaning and testing*, Journal of testing and evaluation **36**, N° 1 (2008).

[12] V. T. Bechel and R. Y. Kim, *Damage trends in cryogenically cycled carbon/polymer composites*, Composites Science and Technology **64** (2004).

[13] L. E. Evseeva an d S. A. Tanaeva, *Thermophysicl properties of epoxy composite materials at low temperatures*, Cryogenics **35**, 4 (1995).

[14] R. P. Reed and M. Golda, *Cryogenic properties of unidirectional composites*, Cryogenics **34**, 11 (1994).

[15] W. N. Reynolds, *Physics Properties of Graphite*, ed. Elsevier, Amsterdam (1968).
[16] Carbon Fiber Society of Japan: *Carbon Fiber-Characteristics and Handling*, revised edition, Tokyo, Carbon Fiber Society of Japan (2000).
[17] T. Kihara, N. Kiuch, T. Komami, O. Katoh, Y. Arai, T. Nakamura, T. Watanabe, G. Ishikawa, Proc. 6th Japan Int. SAMPE Symposium, p. 1131-1134 (1999).
[18] S. Gustavsson, E. Karawacki and N. Khan, *Determination of the thermal-conductivity tensor and the heat capacity of insulating solids with the transient hot-strip method*, J. Appl. Phys. **52**, 2596 (1981).
[19] M. Gustavsson, E. Karawacki and E. Silas, *Thermal conductivity, thermal diffusivity, and specific heat of thin samples from transient measurements with hot disk sensors*, Rev. Sci. Instrum. **65**, 3856 (1994).
[20] V. Bohac, M. K. Gustavsson, L. Kubicar and S. E. Gustafsson, *Parameter estimations for measurements of thermal transport properties with the hot disk thermal constants analyser*, Rev. Sci. Instrum. **71**, 2452 (2000).
[21] Y. He, *Rapid thermal conductivity measurement with a hot disk sensor: Part 1. Theoretical considerations*, Thermochimica Acta **436**, Issues 1–2 (2005).
[22] X. Zhang, S. Fujiwara and M. Fujii, *Measurement of thermal conductivity and electrical conductivity of a single carbon fiber*, International Journal of Thermophysics, **21**, N°4 (2000).
[23] T. Pérez-Castañeda, J. Azpeitia, J. Hanko, A. Fente, H. Suderow and M. A. Ramos, *Low-temperature specific heat of graphite and CeSb2: Validation of a quasi-adiabatic continuous method*, Journal of Low Temperature Physics.
[24] Klemens, P. G., *The Specific Heat and Thermal Conductivity of Graphite*, Australian Journal of Physics **6**, p.405 (1953).